Supporting Information

Three-Dimensional Super-Resolution Imaging of Single Nanoparticle Delivered by Pipettes

Yun Yu[†,‡], Vignesh Sundaresan[†,‡], Sabyasachi Bandyopadhyay[†], Yulun Zhang[§], Martin A. Edwards[§], Kim McKelvey[§], Henry S. White[§], and Katherine A. Willets*[,†]

[†]Department of Chemistry, Temple University, Philadelphia, Pennsylvania 19122, United States

[§]Department of Chemistry, University of Utah, Salt Lake City, Utah 84112, United States

Corresponding Author

Katherine A. Willets, e-mail: kwillets@temple.edu.

Table of Contents
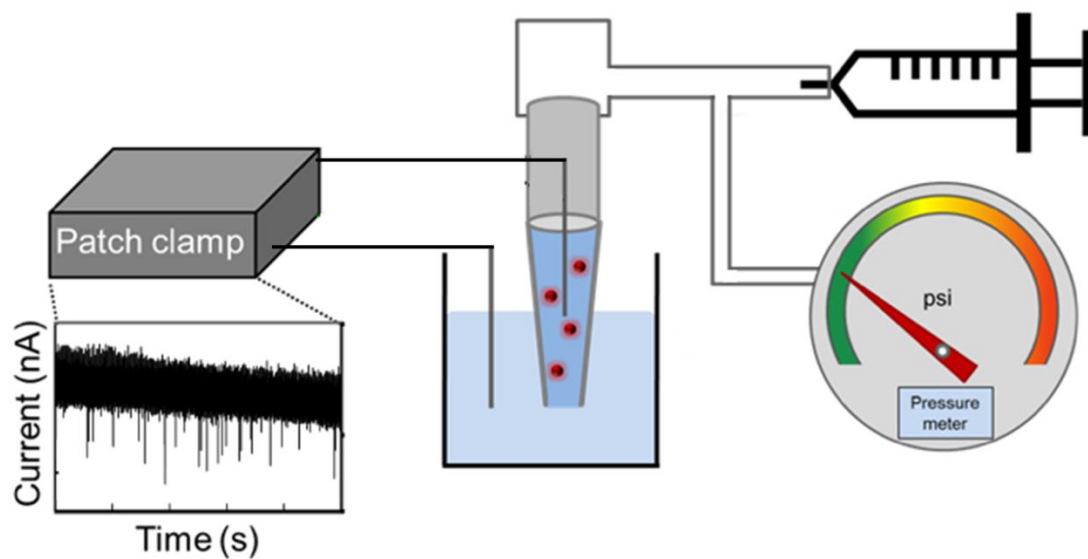
1. Resistive-pulse setup

Figure S1. Schematic representation of the setup for resistive-pulse measurements. The electrolyte-filled pipette, connected to a syringe and a pressure meter, is immersed in electrolyte in an electrochemical cell. One Ag/AgCl wires is placed in the internal solution and another in the external solution. The ionic current flowing between the two quasi-reference electrodes is recorded with a patch clamp amplifier. For clarity the microscope, Faraday cage, stepper motors and piezoelectric positioners are omitted.

2. Characterization of the pipettes.

The geometries of the pipettes were characterized using scanning electron microscopy (SEM). The ionic current-voltage curve of the pipette shows behavior close to that of a typical resistor, although a small amount of current rectification occurs due to the negative charge on the pipette wall.
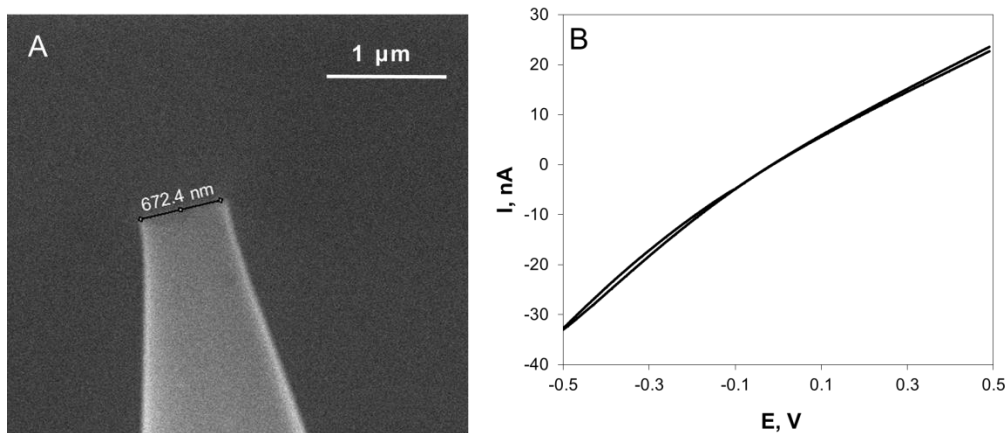

Figure S2. (A) SEM image of a nanopipette with diameter of 672 nm. (B) The current-voltage response of the same nanopipette in 50 mM buffer solution (20 mM NaH_2PO_4 and 30 mM Na_2HPO_4, pH 7.1). The scan rate was 50 mV/s.

3. Simulated resistive-pulse response.

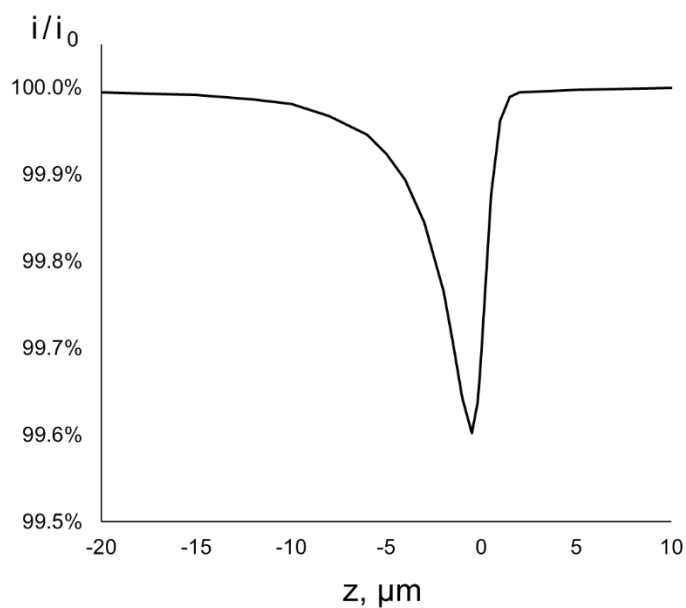**Figure S3.** Simulated resistive pulse of a 270-nm-radius particle translocating through the orifice of a 1-μm-radius pipette. z=0, z>0, and z<0 correspond to the NP located at the pipette orifice, outside and inside pipette, respectively. i_0 is the ionic current when the particle is far away from orifice. Surface charge on glass or particle is not incorporated in the simulation (for details of simulations, see section S11).

4. The effect of the applied pressure to the particle translocation frequency.
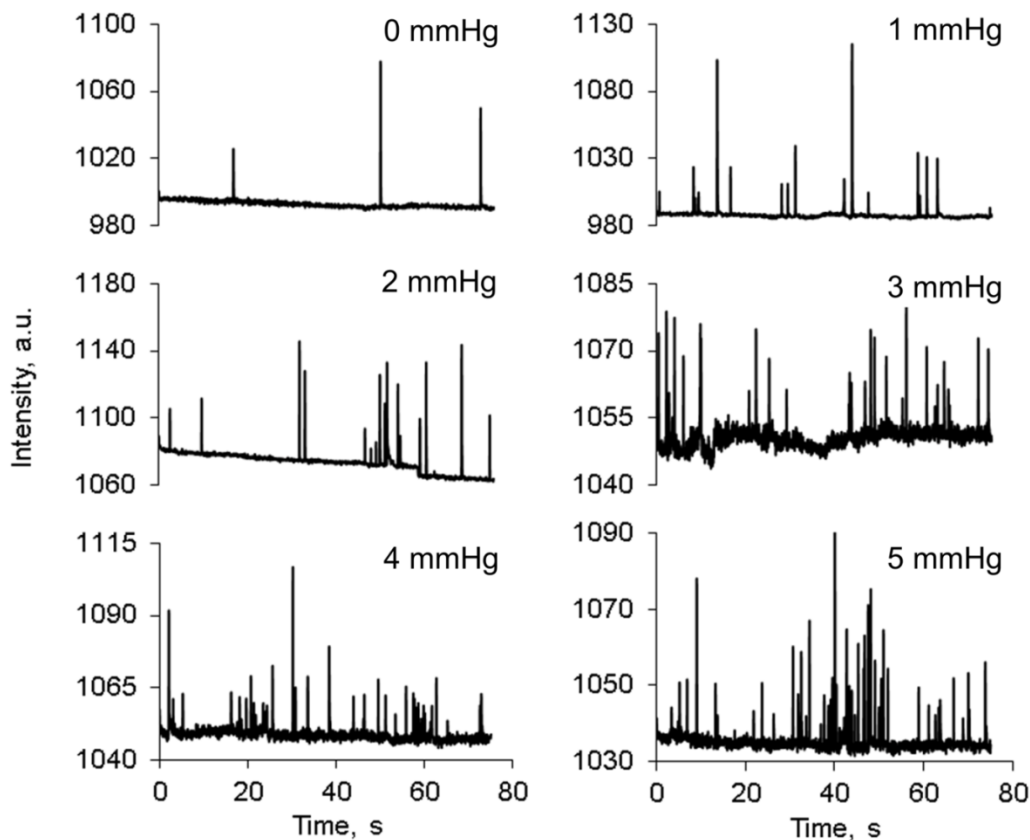

Figure S4. Traces of optical intensity at the pipette orifice vs. time for particles leaving the pipette under different applied pressures (labelled). Solution containing 130-nm-radius NPs was filled inside a 1-μm-radius pipette.

5. Nanopipette positioning in a delivery experiment.

The pipette was first manually positioned at a vertical distance of ca. 10 μm from the substrate and monitored optically. The electrochemical cell was then filled with buffer solution. The nanopipette was slowly brought towards the surface using a piezo actuator (10 nm/step) while the ionic current was recorded and used as the feedback response to determine the nanopipette-substrate distance. A typical ionic current-distance plot is shown in Figure S5. The decrease of the current by ~4% indicates that the pipette is 1-2 pipette radii from the substrate when d=6.4 μm.
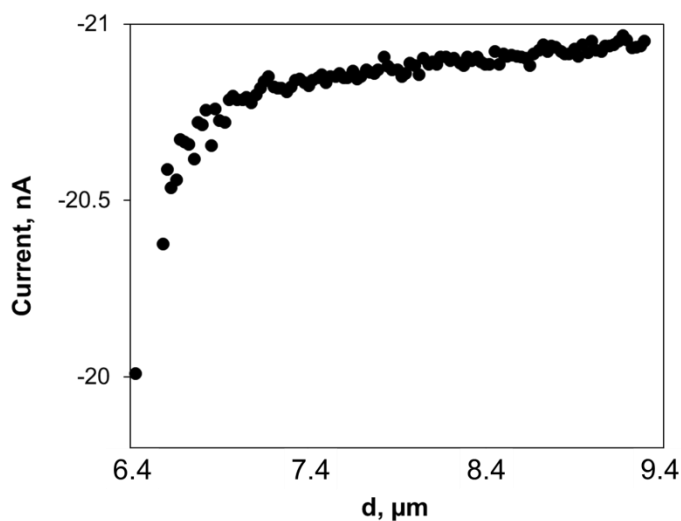

Figure S5. Current vs pipette displacement curve of a 280-nm-radius pipette approaching to a glass substrate.
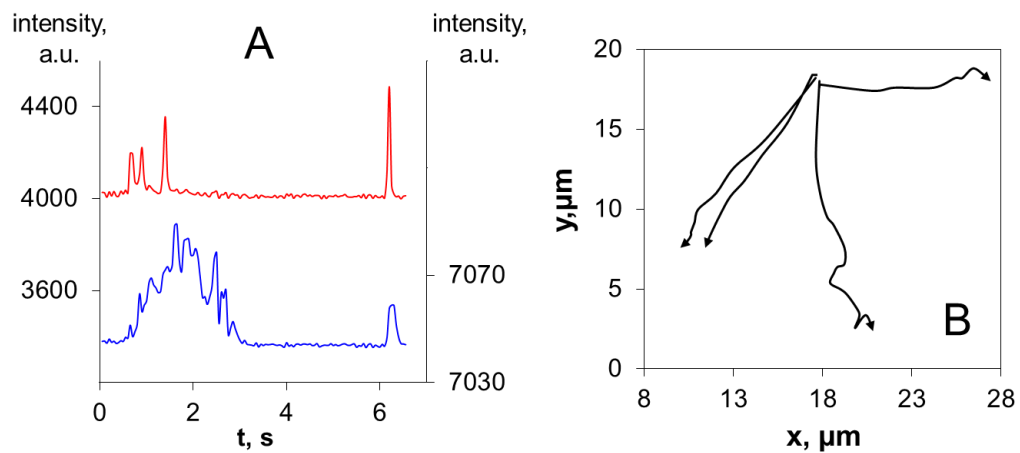
6. NP behavior at $E_{ITO}=0.8$ V.

Figure S6. (A) Optical intensity vs time as assessed at the pipette orifice (red) and the underlying ITO surface (blue) for the delivery of 4 130-nm-radius nanoparticles from a pipette. (B) The *x-y* trajectories of the 4 NPs in panel A. 1 mmHg differential pressure was applied to the pipette and the ITO was poised at $E_{ITO}=0.8$ V vs Ag/AgCl.
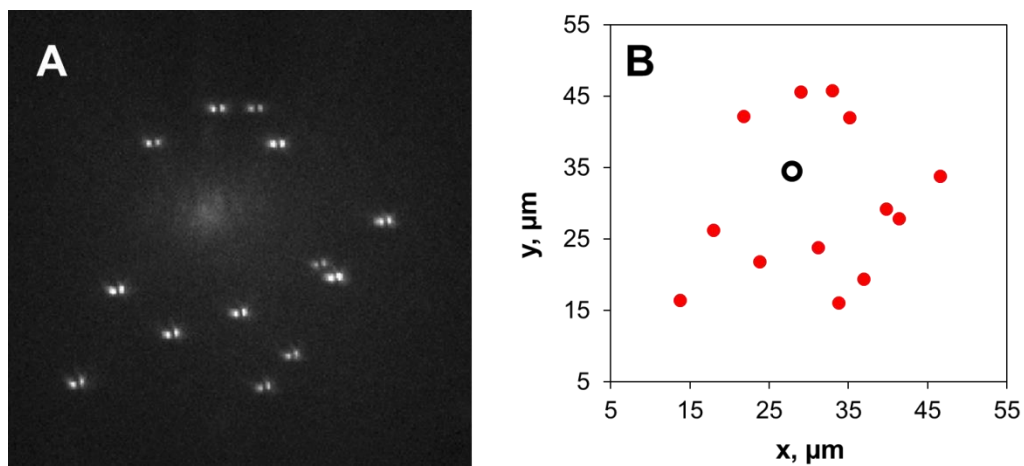
7. NP deposition at $E_{ITO}=1.4$ V.

Figure S7. (A) Optical images of 13 130-nm-radius NPs immobilized after delivery from a pipette to an ITO surface poised at 1.4 V vs Ag/AgCl. (B) The positions of the NPs (red points) and the pipette (black circle) extracted from panel A. See section 10 for details of image analysis.
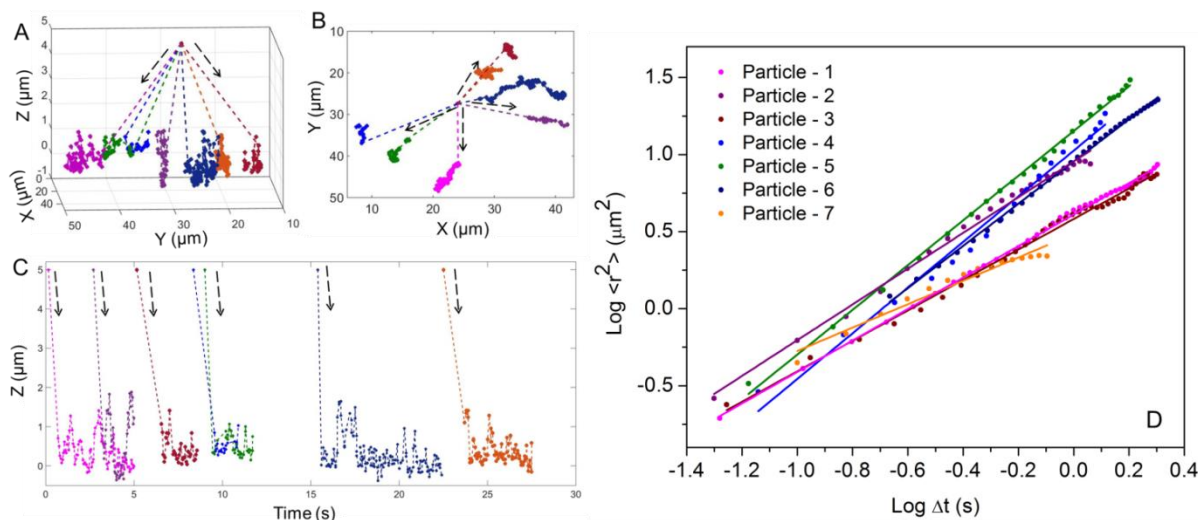
8. NP behavior at E_{ITO}=1V.

Figure S8. (A) 3-D trajectories of 7 NPs (130-nm-radius) delivered by a 1-μm-radius pipette to an ITO surface with E_{ITO}=1 V vs Ag/AgCl. (B) *x-y* trajectories and (C) *z-t* plots of the same particles. (D) Plots of the mean squared displacement vs time from delivery (points) and linear fits to these data (lines).

Table S1. *α* and *D* values of the 7 NPs obtained by linear fitting of the power law (Equation 2 in main text) to the data shown in Figure S8, part D.

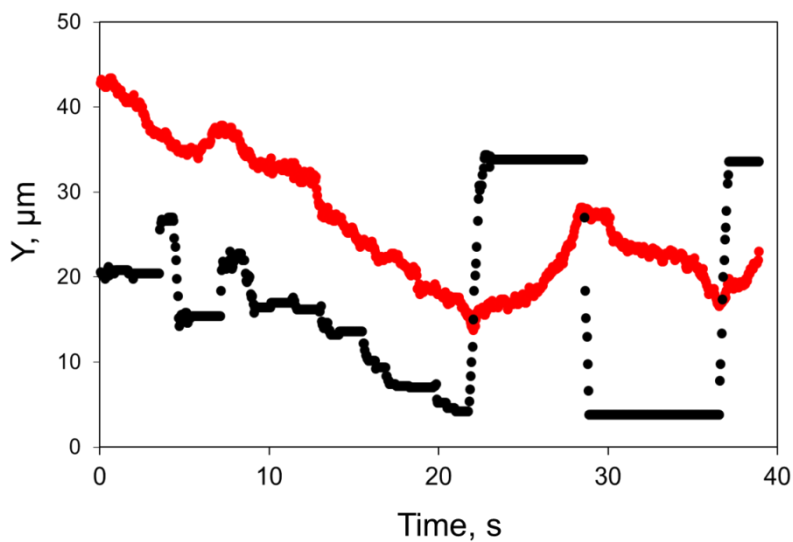|	*α*	*D* ($μm^2$/s)
1	1.18	0.76
2	1.16	1.51
3	0.99	0.64
4	1.48	1.77
5	1.45	2.37
6	1.46	1.46
7	0.67	0.40

9. Manipulation of the NP trajectory.

Figure S9. The trajectory of a moving pipette (1-µm-radius, black dots) and a 130-nm-radius NP in the external solution (red dots). A negative differential pressure (-1 mmHg) was applied and E_{ITO}=1 V. The pipette was manually shifted along the y-axis. The NP was essentially following the pipette trajectory.

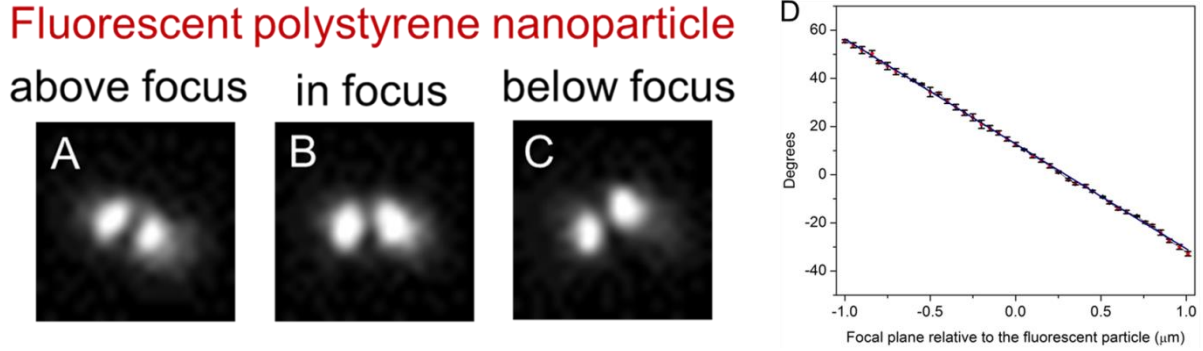## 10. Three-dimensional super-resolution imaging.

Figure S10. Double helix optical image of a 130-nm-radius fluorescent polystyrene particle showing different angles between the lobes when the particle is placed above (A), on (B) and below (C) the focal plane of the objective. (D) Optical calibration curve shows the degrees between the two lobes as a function of the relative position of the focal plane from the fluorescent particle.

The precision in the z-position was determined by, first calculating the uncertainty for the y variable (S_y) in the calibration curve (Figure S10D) and secondly, solving the uncertainty in the x value (S_x) using the following equation

$$s_x = \frac{s_y}{m}\sqrt{\frac{1}{k}+\frac{1}{n}+\frac{(y-\bar{y})^2}{m^2\sum(x_i-\bar{x})^2}} \tag{S-1}$$

where,

S_y - Uncertainty in the y variable ($S_y = \sqrt{\frac{\Sigma(yi-y)^2}{n-2}}$)

m – Slope of the calibration curve

k – Number of measurements in unknown sample

n – Number of points in calibration curve

y - Value of unknown

$\bar{y}$ – Average y-value of calibration curve points

X_i – Values of x data on calibration curve

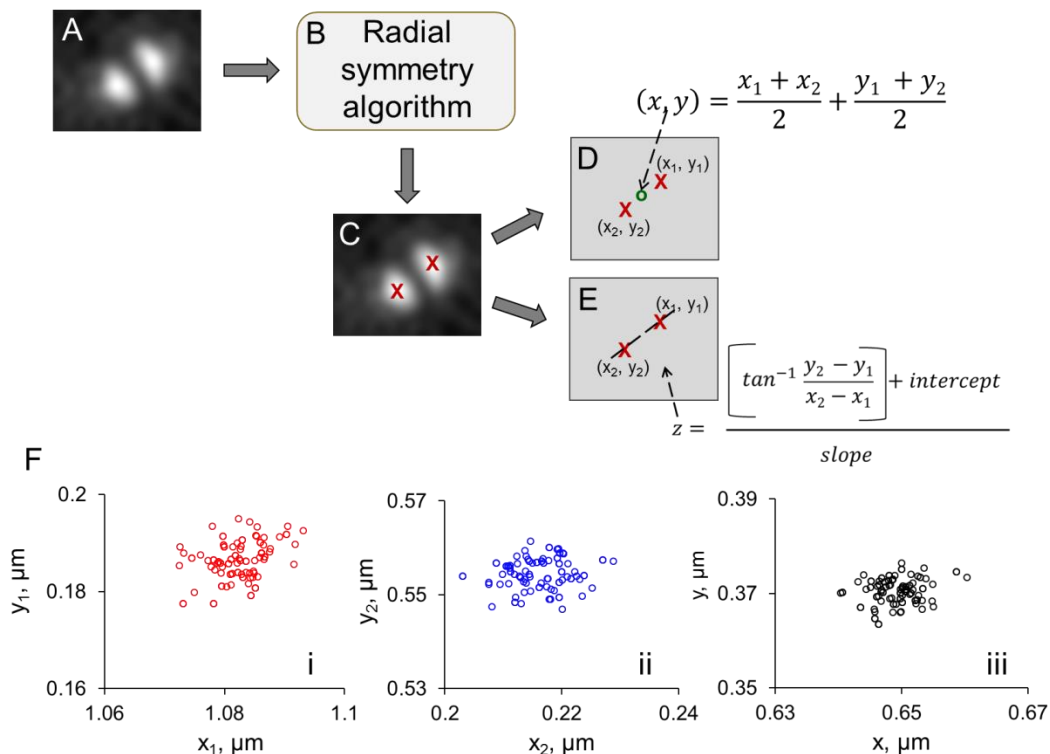$\bar{X}$ – Average x-value of calibration curve points

Figure S11. Schematic showing the process of obtaining 3-D coordinates of an NP. (A) Example of a double-helix image of a single NP with the two lobes. (B) Fitting the optical image (S11-A) using a Radial symmetry algorithm. (C) The center positions (marked in red ×) of the two lobes in a double-helix image. (D) Schematics of obtaining the lateral coordinates (x and y). (E) Schematics of obtaining the axial coordinates (z). (F) x-y coordinates obtained from the fitting of 100 images of a stationary marker. The positions of the left lobe, the right lobe and the average of the two lobes are shown in panels i, ii and iii, respectively. The standard deviation is 5 nm.

11. Finite-element simulations.

COMSOL Multiphysics (version 5.3) was used to compute the pressure and velocity profile across the nanopipette orifice by solving the Navier–Stokes equation for incompressible flow,

$$u\nabla u - \frac{\eta}{\rho}\nabla^2 u + \frac{\nabla p}{\rho} = 0 \qquad (\text{S-2})$$

where u is the velocity and p is the pressure. The model geometry and the boundary conditions are shown in Figure S12. The fluid density ($\rho = 10^{-3}$ kg·m^{-3}) and viscosity ($\eta = 8.9 \times 10^{-4}$ Pa·s) corresponding to aqueous solutions were used. Gravitational forces, which should be minimal on this length-scale, are ignored. The contribution of the electroosmotic forces to the flow was also ignored as in the experiments in this work pressure-driven flow dominates.

Two different configurations were used for modelling where the pipette was considered in the presence (Figure S13) or absence (Figure S12) of an interface or particles.
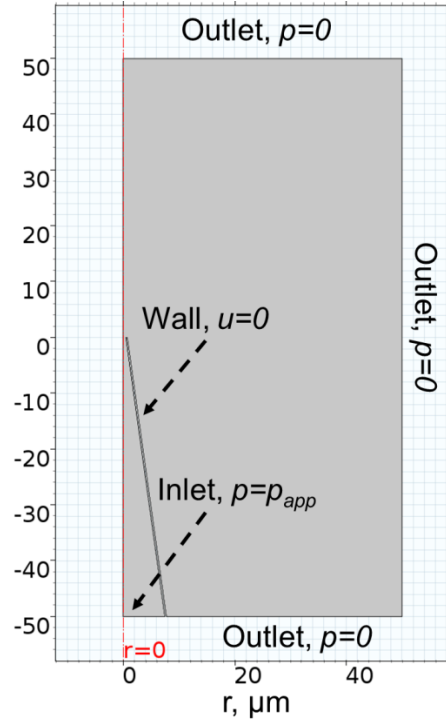

Figure S12. Model geometry in the absence of a surface/particle and the boundary conditions. p_{app} represents the pressure applied to the pipette.
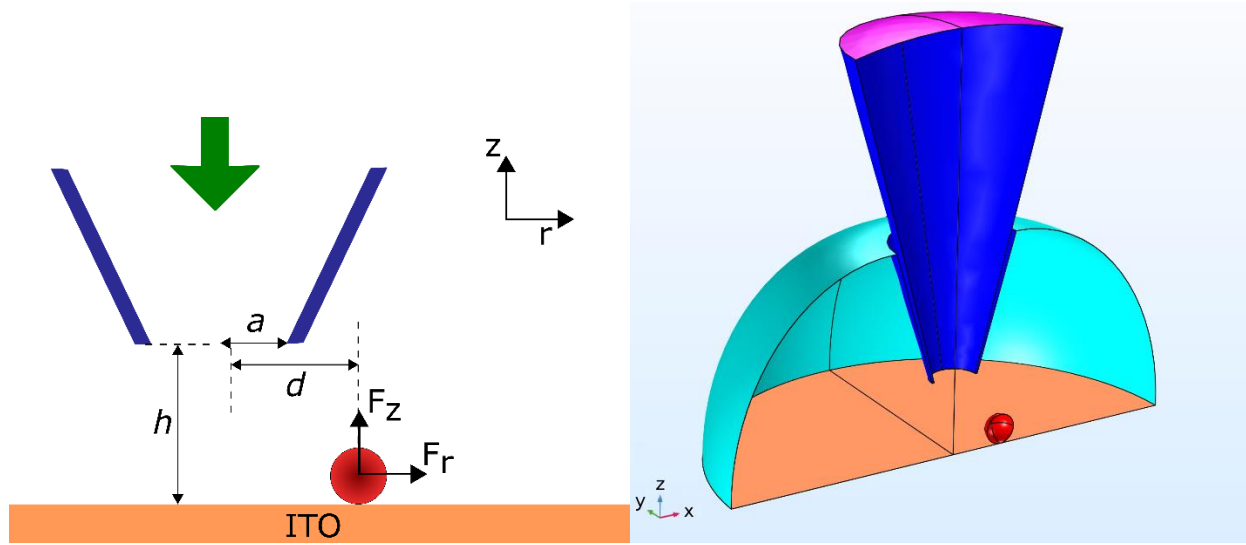
Figure S13. The left panel is the schematic of the geometry used for finite element modelling of the hydrodynamic forces on a particle on as surface. Geometric parameters and the radial (F_r) and lateral (F_z) components of the force on the particle are shown. The right panel is the plot of the half of the 3-dimensional domain used for simulations. The boundaries representing the glass (blue), external solution (cyan), particle (red), ITO surface (orange) and internal solution (magenta) are all shown, while the symmetry (*x-z*) plane is not shown.

Boundary Conditions

A no-slip condition boundary condition ($\underline{u}=0$) was applied on the surface or the particle (red boundary in Figure S13), the pipette (blue) and on the ITO surface (orange). The plane of symmetry was set to satisfy a 'no normal flow' condition

$$\underline{u} \cdot \vec{n} = 0 \qquad \text{(S-3)}$$

Where $\vec{n}$ is the inward pointing unit normal.

The external solution (cyan) was set at a reference pressure of $p = 0$, while the boundary with the internal solution (magenta in Figure S13) was set at a pressure to match that used in the experiments, p_{app}. In each case the velocity is restricted to being in the direction normal to the interface.

Meshing

The domain of simulation was discretized by a mesh. In all cases the mesh size at the conical orifice and near the particle (where simulated) was refined to obtain more accurate simulation results. An example mesh is shown in Figure S14.
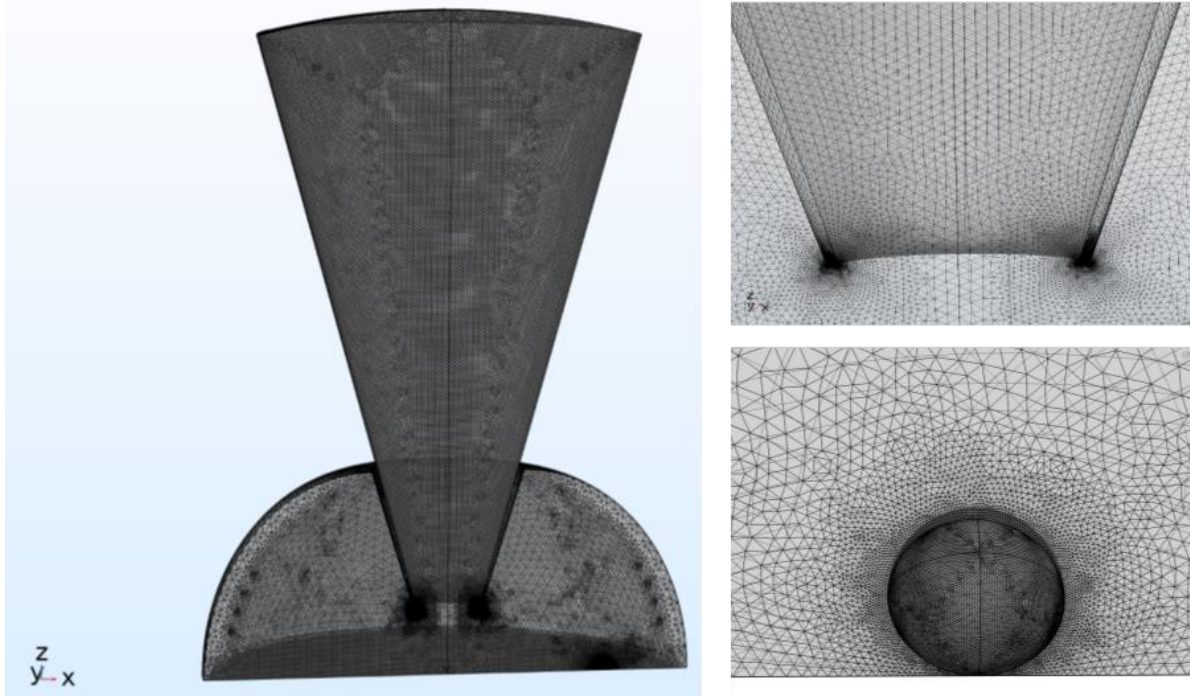

Figure S14. Example mesh used for finite element simulations, including zoom-ins around the orifice (top-right) and particle (bottom-right).

Forces

The components of the force on the particle in the radial and vertical directions were calculated by integration of the product of the pressure and the component of the unit normal to surface of the particle over its surface. These numbers were doubled to take into account the contribution from the mirror image of the sphere which was not simulated.

$$F_r = 2 \int_{half\,particle} p \cdot n_x \qquad \text{(S-4)}$$

Current Calculations

The ionic current during a particle translocation was calculated by solving the Nernst-Plank equation,

$$D_i \nabla c_i + \frac{z_i F}{RT} D_i c_i \nabla \phi - c_i u = 0 \qquad \text{(S-5)}$$

where D_i, c_i, and z_i are the diffusion coefficient, concentration, and charge of species i in solution. ϕ and u are the local electric potential and fluid velocity, and F, R, and T are Faraday's constant, the gas constant, and the temperature, respectively. In the simulation, $D=2\times10^{-5}$ cm^2/s, and $z=\pm1$. The local electric potential, ϕ, was calculated by solving Poisson's equation,

$$\nabla^2 \phi + \frac{F}{\varepsilon} \sum z_i c_i = 0 \qquad \text{(S-6)}$$

where ε ($\varepsilon=80\varepsilon_0$) is the dielectric constant of the solution. The effect of surface charge on the glass and the particle was ignored. The current was evaluated by the surface integration of the total ion flux at the internal electrode. The model geometry and the boundary conditions are shown in Figure S13.
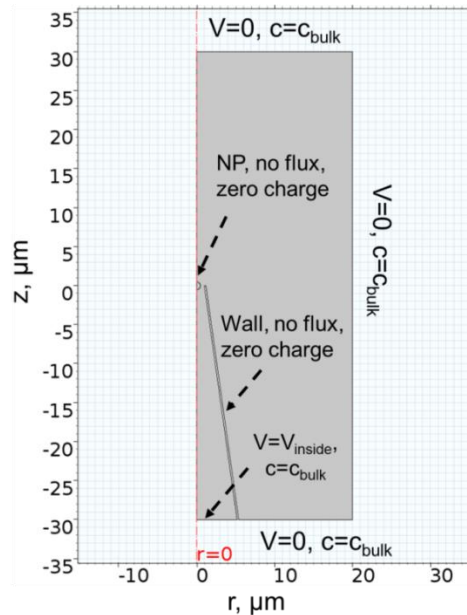

Figure S15. Model geometry and the boundary conditions. V_{inside} represents the electric potential at the inside reference electrode. c_{bulk} represents the bulk concentration of the ion.